Spectroscopic characterization of model compounds, reactants, and byproducts connected with an isocyanate production chain

Emma K. Gibson, June Callison, John M. Winfield, Andrew Sutherland, Robert H. Carr, Archie Eaglesham, Stewart F. Parker and David Lennon

Published version information

Citation: EK Gibson et al. "Spectroscopic characterization of model compounds, reactants, and byproducts connected with an isocyanate production chain." Industrial & Engineering Chemistry Research vol. 57, no. 22 (2018): 7355-7362.

DOI: 10.1021/acs.iecr.8b00853

Paper for submission to: **Industrial Engineering Chemistry Research**

Spectroscopic Characterisation of Model Compounds, Reactants and By-products Connected with an Isocyanate Production Chain

Emma K. Gibson,[a] June Callison,[a] John M. Winfield,[a] Andrew Sutherland,[a] Robert H. Carr,[b] Archie Eaglesham,[b] Stewart F. Parker [c] and David Lennon[a]*

[a] School of Chemistry, Joseph Black Building, University of Glasgow, Glasgow, G12 8QQ, UK.

[b] Huntsman (Europe) BVBA, Everslaan 45, 3078 Everberg, Belgium

[c] ISIS Facility, STFC Rutherford Appleton Laboratory, Chilton, Didcot, OX11 0QX, UK

Abstract

Aromatic amines and amine hydrochloride salts play an important part in certain large-scale isocyanate production chains. For the first time, via a combination of periodic-DFT calculations, infrared spectroscopy and inelastic neutron scattering, this work provides a comprehensive vibrational assignment of 4-benzylaniline ($C_6H_4CH_2C_6H_4NH_2$), 4,4'-methylenedianiline ($H_2NC_6H_4CH_2C_6H_4NH_2$) and their associated amine hydrochloride salts. Deuterated analogues are additionally utilised to assist vibrational assignments. The heightened awareness of vibrational transitions for these technically relevant reagents and by-products provides the opportunity to apply infrared spectroscopy as an in-line diagnostic tool within the industrial-scale process operation.

Keywords:

4-benzylaniline, 4,4'-methylenedianiline, vibrational spectroscopy, infrared spectroscopy, inelastic neutron scattering, periodic DFT calculations, methylene diphenyl diisocyanate production chain.

1. Introduction

Polyurethanes are used extensively within modern society, having applications in diverse areas such as construction, automotive components, and insulation. Polyurethanes are typically prepared by the reaction between an isocyanate and a diol. [1] Methylene diphenyl diisocyanate (MDI, $OCNC_6H_4CH_2C_6H_4NCO$) dominates the global isocyanate market; in 2011 the MDI total production capacity was estimated to be ~5 Mt.[2]

The large-scale production of MDI can be achieved by phosgenation of 4,4'-methylenedianiline (MDA, $H_2NC_6H_4CH_2C_6H_4NH_2$). This can be envisaged as a two-step process, where phosgenation of the amine initially forms a carbamoyl chloride that subsequently decomposes to form the desired isocyanate (Equations 1 and 2).

$$RNH_2 + COCl_2 \rightarrow RNHC(O)Cl + HCl \quad (1).$$

$$RNHC(O)Cl \rightarrow RNCO + HCl \quad (2).$$

The unit operation is complicated by the hydrogen chloride by-product of the phosgenation reaction. This leads to protonation of the aromatic amine starting material to form an unwanted hydrochloride salt, Equation 3.

$$RNH_2 + HCl \rightarrow RNH_3Cl \quad (3).$$

The amine hydrochloride salt constitutes a source of yield loss within the process, which can be minimised by a further phosgenation stage that returns the desired isocyanate, Equation 4.

$$RNH_3Cl + COCl_2 \rightarrow RNCO + 3HCl \quad (4).$$

In the large-scale process, the R group represents a mixture consisting of a homologous series of isomeric forms of various methylene-bridged poly(aryl) poly(amine) moieties. These reactions take place using a process solvent, typically chlorobenzene (C_6H_5Cl).[2]

Gibson and co-workers have previously studied the hydrochlorination of 4,4'-methylenedianiline in chlorobenzene, providing a structural and spectroscopic awareness of the formation of the dihydrochloride salt, 4,4'-methylenedianiline dihydrochloride (MDA.2HCl, $[H_3NC_6H_4CH_2C_6H_4NH_3]Cl_2$). In certain circumstances a monohydrochloride salt (MDA.HCl) can be isolated.[3] Earlier work from Gibson *et al*. also investigated the hydrochlorination of 4-benzylaniline (4-BA, $C_6H_4CH_2C_6H_4NH_2$) in chlorobenzene.[4] 4-Benzylaniline constitutes a model aromatic amine which, although simpler in function than the diamine and polyamine starting materials used in the commercial process is, nevertheless, representative of molecules encountered in the large-scale process environment. 4-BA therefore constitutes a useful reference reagent when considering how mass may be partitioned during certain isocyanate manufacturing processes.

A major feature of these previous studies of 4-BA and MDA was the use of infrared spectroscopy to characterise the various compounds encountered within the hydrochlorination process. Given the amenability of applying infrared spectroscopy within an actual process environment,[5] it is important that the origins of the particular bands of certain molecules are established. However, some of the vibrational bands have non-trivial origins. For example, 4-BA.HCl possesses an intense broad feature about 2600 cm^{-1} that is attributed to a Fermi resonance interaction between a symmetric deformation NH_3 mode at 1527 cm^{-1} and a NH_3 rocking mode at 1075 cm^{-1}.[4] Similar spectral complexity is equally evident in the manifold of MDA derived entities.[3]

Against this background, it is timely to undertake a complete vibrational analysis of molecules connected to the hydrochlorination of 4-BA and MDA. To date, no such comprehensive database is available. In order to assist peak assignments, deuterated analogues of various entities were additionally explored. Figure 1 presents the molecules examined in the present

study. The 4-BA manifold of molecules comprises 4-BA (**1**), 4-BA.HCl (**2**), deuterated 4-BA (4-BA-D2, **3**) and 4-BA.DCl (**4**), the deuterated analogue of the hydrochloride salt. The MDA manifold of molecules comprises MDA (**5**), the monohydrochloride MDA.HCl (**6**), the dihydrochloride MDA.2HCl (**7**), deuterated MDA (MDA.D4, **8**) and MDA.2DCl (**9**), the deuterated analogue of the hydrochloride salt.

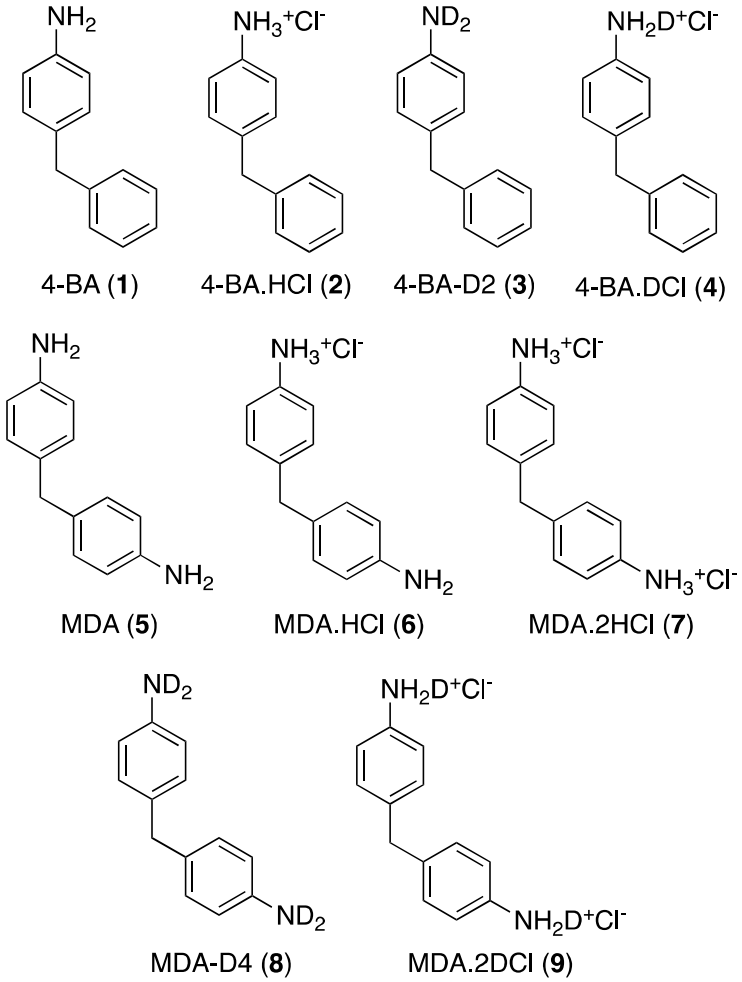

Figure 1. The 4-BA manifold of molecules: 4-BA (**1**), 4-BA.HCl (**2**), deuterated 4-BA (4-BA-D2, **3**) and 4-BA.DCl (**4**), the deuterated analogue of the hydrochloride salt. The MDA manifold of molecules: MDA (**5**), the monohydrochloride MDA.HCl (**6**), the dihydrochloride MDA.2HCl (**7**), deuterated MDA (MDA.D4, **8**) and MDA.2DCl (**9**), the deuterated analogue of the hydrochloride salt.

The work described here uses the atomic coordinates from the previously reported single crystal XRD data collected for 4-BA and 4-BA.HCl, MDA and its mono and dihydrochloride salts[3,4] as inputs for *ab initio* studies. The atomic displacements calculated from these studies are then used to predict the inelastic neutron scattering (INS) spectra,[6] which are compared with experimentally obtained INS spectra for each compound. An advantage of INS spectroscopy is its ability to measure low wavenumber vibrational modes. This is especially useful for amine and amine hydrochloride salts, as the N–H torsional mode, $\tau(NH_x)$, occurs in this region, the position of which is characteristic for these species.[7,8] The resulting comprehensive vibrational analysis then facilitates the application of infrared and/or Raman spectroscopy as diagnostic probes suited to application in the process environment.

2. Experimental

The amines, 4-benzylaniline (4-BA, 98 %, Alfa-Aesar) and 4,4'-methylenedianiline (MDA, 97 %, Sigma-Aldrich) were used for characterisation without further purification. The preparation of the hydrochloride salts is described in detail elsewhere,[3,4] but primarily consisted of bubbling anhydrous $HCl_{(g)}$ through a solution of the amine in chlorobenzene which had been previously degassed by purging with $N_{2(g)}$. The preparation of the monohydrochloride MDA.HCl was more complicated and involved transferring a stoichiometric amount of $HCl_{(g)}$ to a Pyrex cell, the HCl was then frozen using an isopentane/liquid N_2 slush bath to allow for controlled addition of a dilute flow of $HCl_{(g)}$ in a $N_{2(g)}$ carrier stream into the MDA solution. This method reproducibly prepared MDA.HCl.[3] MDA.HCl (**6**) is unusual in that two structural motifs are observed. The stoichiometry of the as-synthesized polycrystalline form is MDA.HCl. However, crystallisation of this material from solutions of MDA.HCl in methanol

were found by X-ray analysis to consist of the basic hydrochloride salt, $[(MDA)_2(MDA.2HCl)(H_2O)]$, which is stabilised by complex hydrogen bonding.[3] The INS spectrum of MDA.HCl (Figure 10) corresponds to polycrystalline MDA.HCl (**6**). The deuterated compound of this salt was not prepared, neither was the INS spectrum of $[(MDA)_2(MDA.2HCl)(H_2O)]$ recorded.

The N-deuterated isotopomers of 4-BA, 4-BA.HCl, MDA and MDA.2HCl were prepared by using a H-D exchange method. Both 4-BA and MDA were dissolved in benzene-D_6 and D_2O was added. The solution was stirred and samples taken over time to be analysed by ^{1}H-NMR spectroscopy. The spectra were recorded on a Bruker Advance spectrometer fitted with a Quattro nucleus probe (QNP) at 400 MHz. The disappearance of the NH_2 peak indicated the production of the deuterated compound. The N-deuterated isotopomers of the hydrochloride salts were prepared in the same manner using chloroform-D_1 as the solvent and monitoring the disappearance of NH_3^+ in the ^{1}H NMR spectra. ^{1}H NMR spectra of 4-BA (**1**), 4-BA-D2 (**3**), 4-BA.HCl (**2**) and 4-BA.DCl (**4**) are presented in Figure S1. ^{1}H NMR spectra of MDA (**5**), MDA-D4 (**8**), MDA.2HCl (**7**) and MDA.2DCl (**9**) are presented in Figure S2.

Infrared analyses of the solids were obtained using ATR-FTIR spectroscopy on a Pike MIRacle ATR accessory with a diamond/ZnSe element used within a purged Nicolet Avatar 360 FTIR spectrometer. Infrared spectra of 4-BA (**1**), 4-BA.HCl (**2**) are presented in Figure S3; infrared spectra of MDA (**5**), MDA.HCl (**6**) and MDA.2HCl (**7**) are presented in Figure S4.

INS spectra were recorded on the TOSCA spectrometer[9] at the ISIS neutron source at the Rutherford Appleton Laboratory, Chilton.[10] Spectra were measured at 20 K using a 24 position sample changer, with samples being folded into aluminium foil packets of 40 × 40 × 1 mm, containing 1-3 g of sample. The spectra are available from the INS database at: http://wwwisis2.isis.rl.ac.uk/INSdatabase/

Periodic density functional theory (DFT) calculations were carried out using a plane wave basis-set and pseudopotentials as implemented in the CASTEP code.[11] As initial inputs, the experimental crystal structures were used.[3,4] The generalised gradient approximation (GGA) Perdew-Burke-Ernzerhof (PBE) functional was used in conjunction with optimised norm-conserving pseudopotentials. The plane-wave cut-off energy and Monkhorst-Pack grids were: 4-BA 770 eV, 3×3×3 (10 k-points), 4-BA.HCl 830 eV, 8×8×4 (64 k-points), MDA 770 eV, 4×4×4 (8 k-points), MDA.HCl 830 eV, 4×4×2 (10 k-points), MDA.2HCl 1000 eV, 6×8×2 (24 k-points), all of the calculations were converged to better than |0.005| eV $Å^{-1}$. After geometry optimisation, the vibrational spectra were calculated in the harmonic approximation using density-functional perturbation-theory.[12] This procedure generates the vibrational eigenvalues and eigenvectors, which allows visualisation of the modes within Materials Studio[13] or Jmol[14] and is also the information needed to calculate the INS spectrum using the program ACLIMAX.[15] Transition energies for isotopic species were calculated from the dynamical matrix that is stored in the CASTEP checkpoint file using the PHONONS utility.[16] We emphasise that none of the transition energies have been scaled.

3. Results

Table 1 compares the observed and calculated geometries of the systems considered here. It can be seen that the significant differences between the data sets are from the X–H (X = C, N, O) distances. Since these were experimentally determined by X-ray diffraction,[3,4] which is well-known to underestimate such distances, the larger calculated distances are more realistic. The experimental variation in the dihedral angle between the aromatic rings between the compounds indicates that it is strongly influenced by the crystal packing. The

ability of the calculations to reproduce this parameter provides confidence in the *ab initio* results.

Relevant to the calculations of the vibrational spectra we note that in the primitive cell of 4-BA (**1**), 4-BA.HCl (**2**) and MDA (**5**) there are four formula units, for MDA.2HCl (**7**) there are two and for $[(MDA)_2(MDA.2HCl)(H_2O)]$ there is only one formula unit. Thus, there is fourfold factor group splitting for 4-BA (**1**), 4-BA.HCl (**2**) and MDA (**5**), twofold for MDA.2HCl (**7**) and none for $[(MDA)_2(MDA.2HCl)(H_2O)]$.

3.1 4-BA, 4BA.HCl and their N-deuterated isotopomers (1-4)

The INS spectra of 4-BA, 4-BA.HCl and their N-deuterated isotopomers in the 0 – 1800 cm^{-1} range are shown in Figure 2. It can be seen that all the spectra are very similar above 600 cm^{-1}, reflecting the commonality of the aromatic framework. The 100 – 550 cm^{-1} region shown in Figure 3 is where most of the modes characteristic of the nitrogen functionality occur, and marked differences are readily apparent both between isotopomers and between the amine and its hydrochloride.

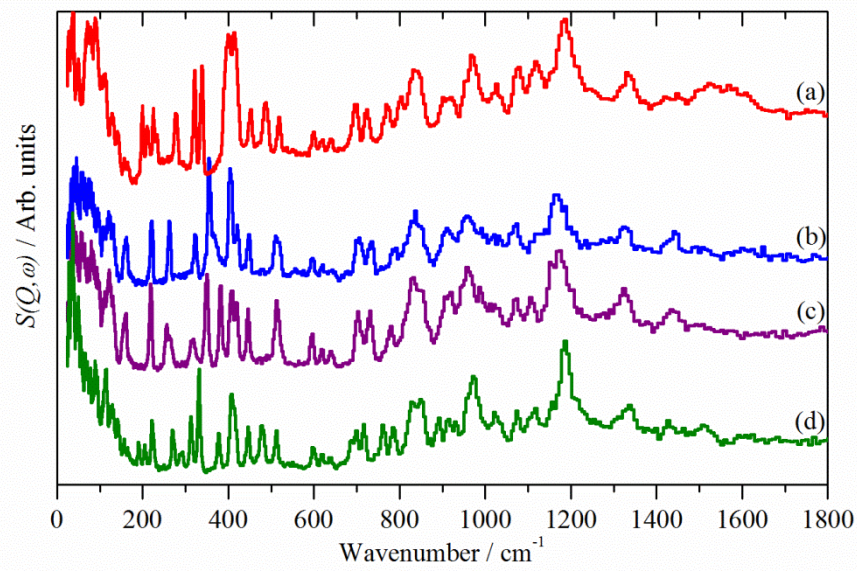

Figure 2. INS spectra of: (a) 4-BA.HCl (**2**), (b) 4-BA (**1**), (c) 4-BA-D2 (**3**) and (d) 4-BA.DCl (**4**) in the 0 – 1800 cm^{-1} range.

A comparison of the observed and calculated INS spectra of 4-BA are shown in Figure 4. The overall agreement is very good, with only two regions of disagreement. The first of these is the 0 – 100 cm^{-1} range. This region includes the dispersed acoustic translational modes as well as optic translational and librational modes, which may also be dispersed. Owing to the size of the unit cell it was only possible to calculate the vibrational transition energies at the Γ-point. Thus the total intensity in this region will be underestimated. (This is also the case for all the other molecules, and their isotopomers, studied here.) The second region is around 400 cm^{-1}, and the reasons for the disagreement are more interesting. Figure 5 shows the observed and calculated spectra for the 200 – 650 cm^{-1} region for 4-BA (**1**) and 4-BA-D2 (**3**) and Figure 6 similarly for 4-BA.HCl (**2**) and 4-BA.DCl (**4**).

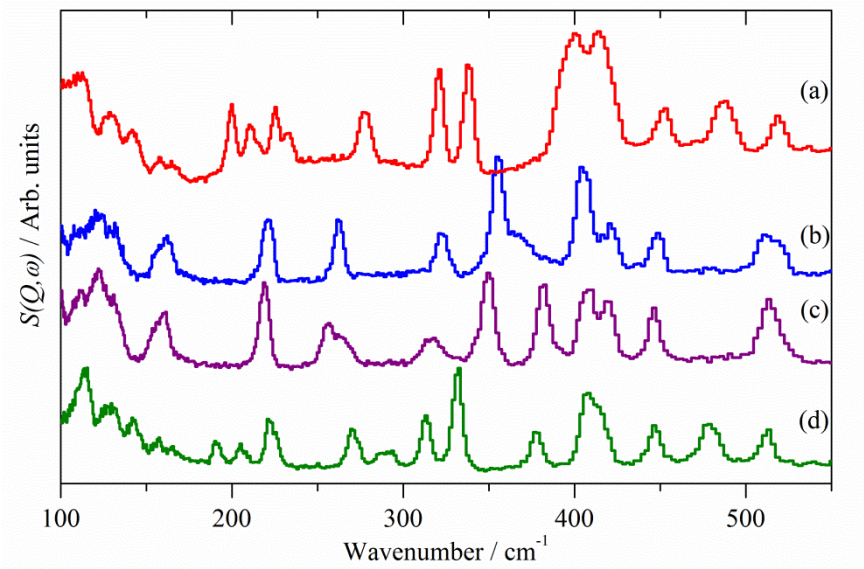

Figure 3. INS spectra of: (a) 4-BA.HCl (**2**), (b) 4-BA (**1**), (c) 4-BA-D2 (**3**) and (d) 4-BA.DCl (**4**) in the 100 – 550 cm^{-1} range.

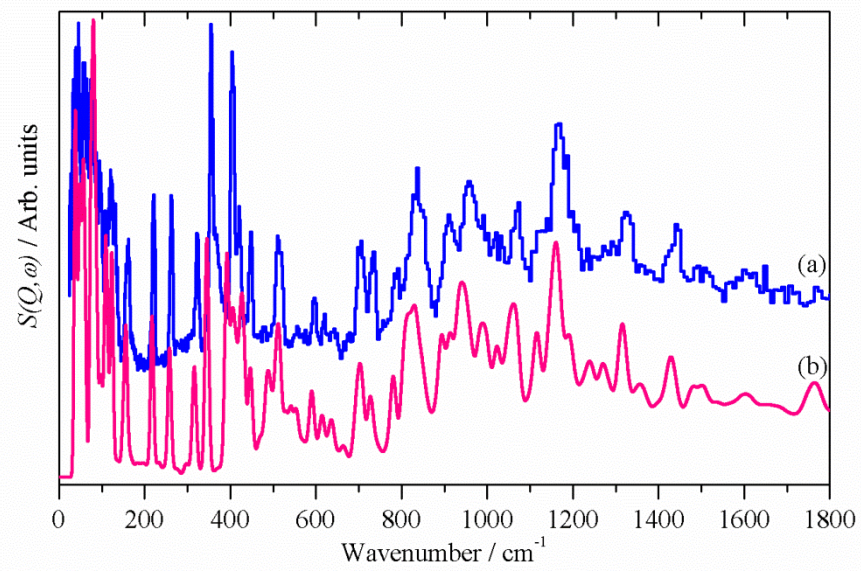

Figure 4. Comparison of: (a) observed and (b) calculated INS spectra of 4-BA (**1**) in the 0 – 1800 cm^{-1} range.

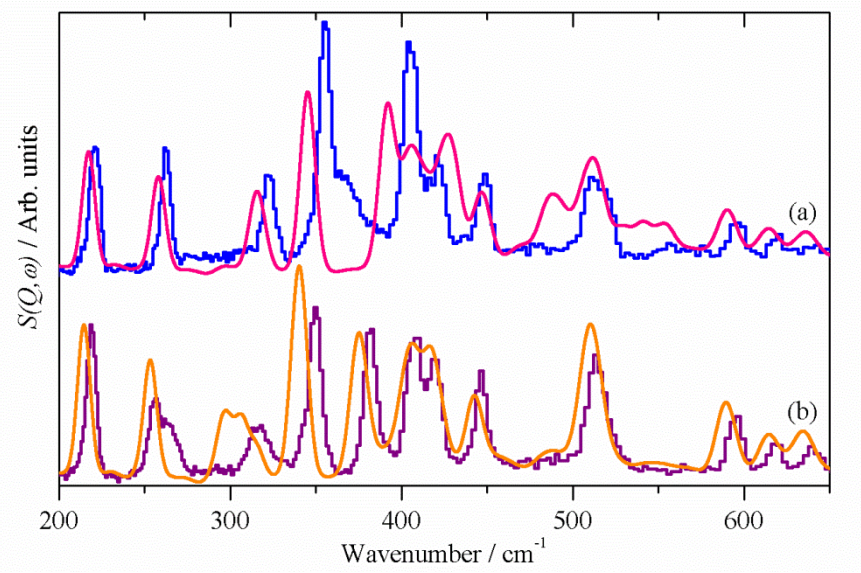

Figure 5. Comparison of observed (histogram plot) and calculated (continuous line) INS spectra of: (a) 4-BA (**1**) and (b) 4-BA-D2 (**3**) in the 200 – 650 cm^{-1} range.

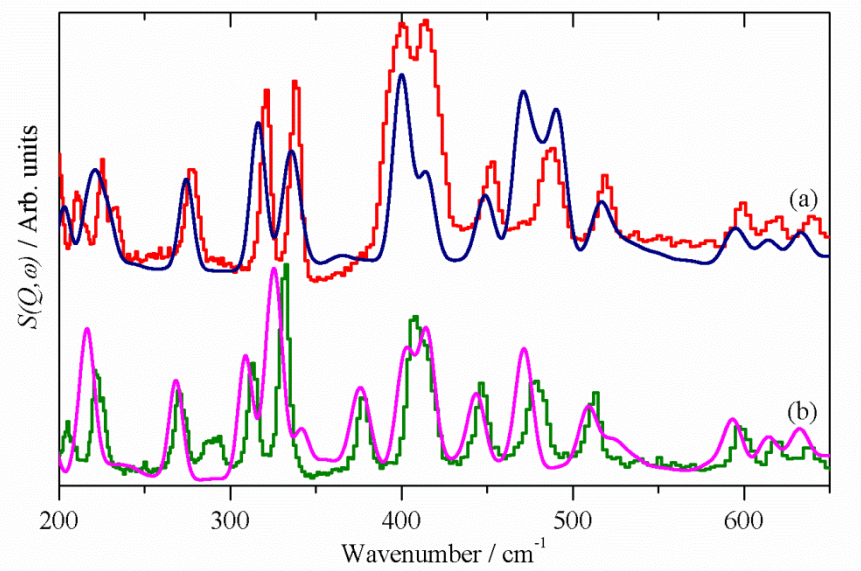

Figure 6. Comparison of observed (histogram plot) and calculated (continuous line) INS spectra of: (a) 4-BA.HCl (**2**) and (b) 4-BA.DCl (**4**) in the 200 – 650 cm^{-1} range.

In both Figures 5 and 6, it can be seen that the agreement between the experimental and calculated spectra is almost exact for the deuterated species, whilst there are significant disagreements in the 350 – 500 cm^{-1} region for the all-hydrogenous species. The reason for this is that the modes that are incorrectly calculated are those that relate to motions of the -NH_x fragment. In the deuterated version, these modes are very weak by virtue of the tenfold smaller cross section of deuterium versus hydrogen, so barely appear in the spectrum and the spectrum is dominated by the modes of the hydrogen atoms attached to the carbon skeleton, which are correctly calculated. The spectroscopic mismatch for the all-H system is useful in that it clearly highlights the -NH_x modes (confirmed by the mode visualisations). Table S1 lists the observed and calculated transition energies for 4BA (**1**) and 4BA-D2 (**3**), while Table S2 lists the same energies for 4BA-HCl (**2**) and 4BA-DCl (**4**).

3.2 MDA, MDA.2HCl and their N-deuterated isotopomers

The results for MDA (**5**), MDA-D4 (**8**), MDA.2HCl (**7**) and MDA.2DCl (**9**) are similar to the corresponding 4-BA compounds. Figure 7 shows INS spectra in the 0 – 1800 cm^{-1} region for all four compounds. Figures 8 and 9 compare the observed and calculated INS spectra for the deformation modes (200 – 650 cm^{-1}) for the four systems. As for the 4-BA materials, the modes are calculated too high in energy for the ^{1}H systems, resulting in the mismatch between observed and calculated spectra, while the agreement is much better for the deuterated compounds. Table S3 lists the observed and calculated transition energies for MDA (**5**) and MDA-D4 (**8**), while Table S4 lists the same energies for MDA-2HCl (**7**) and MDA-2DCl (**9**).

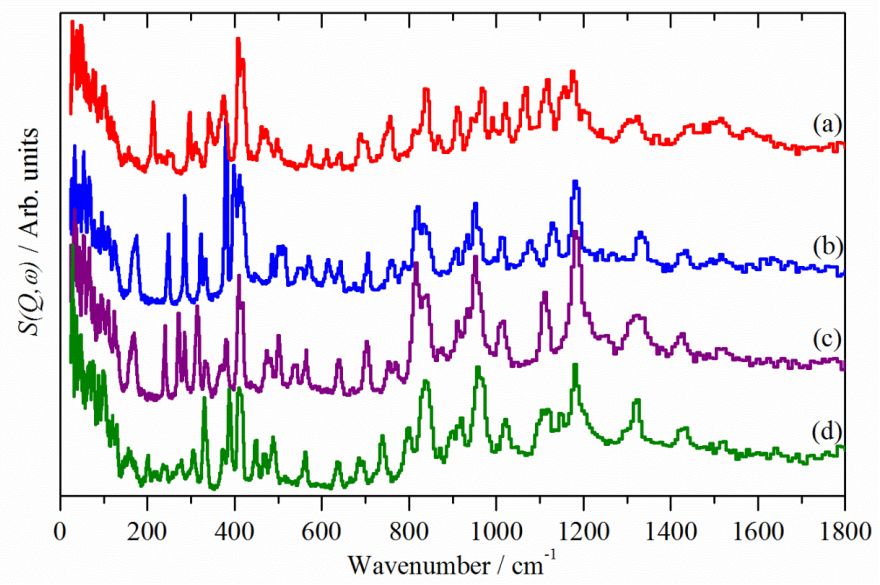

Figure 7. INS spectra of: (a) MDA.2HCl (**7**), (b) MDA (**5**), (c) MDA-D4 (**8**) and (d) MDA.2DCl (**9**) in the 0 – 1800 cm^{-1} range.

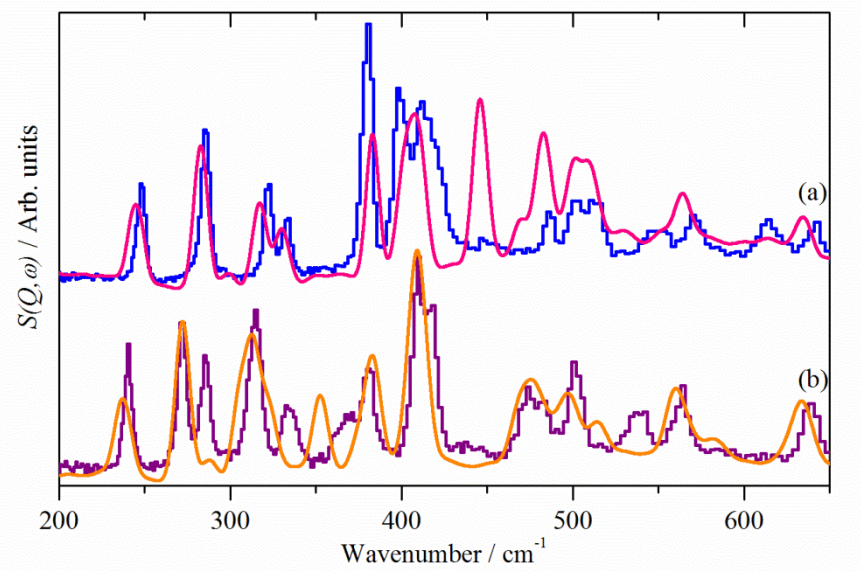

Figure 8. Comparison of observed (histogram plot) and calculated (continuous line) INS spectra of: (a) MDA (**5**) and (b) MDA-D4 (**8**) in the 200 – 650 cm^{-1} range.

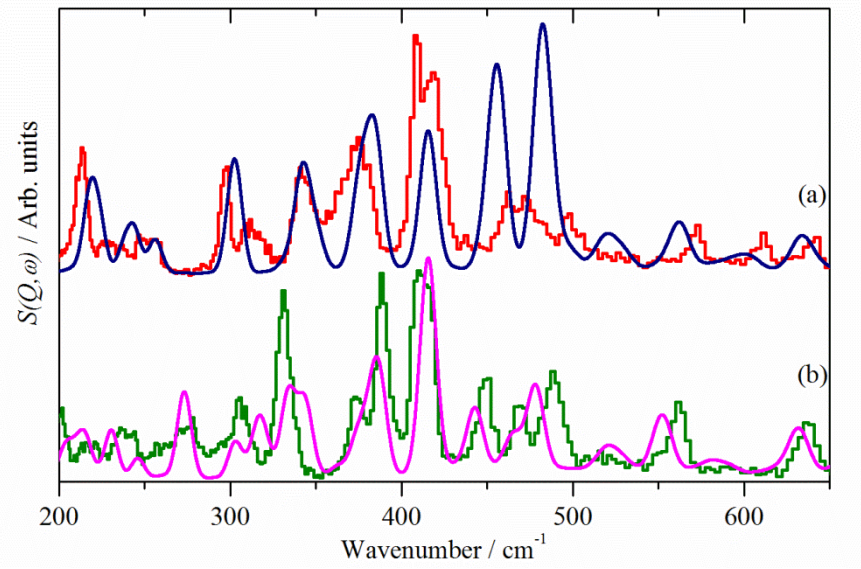

Figure 9. Comparison of observed (histogram plot) and calculated (continuous line) INS spectra of: (a) MDA.2HCl (**7**) and (b) MDA.2DCl (**9**) in the 200 – 650 cm^{-1} range.

3.3 MDA.HCl (6)

As mentioned in the Experimental section, only the INS spectrum for the polycrystalline MDA.HCl was recorded and this is presented in Figure 10(a). However, the simulated INS

spectrum (Figure 10(b)) utilises structural coordinates corresponding to the crystalline hydrochloride salt, $[(MDA)_2(MDA.2HCl)(H_2O)]$, that is stabilised by complex hydrogen bonding.[3] In order to help better understand these spectra, Figure 10(c) also presents a spectrum of water in the 0-1800 cm^{-1} range. The agreement between MDA.HCl and $[(MDA)_2(MDA.2HCl)(H_2O)]$ is understandably not ideal because there are two types of $-NH_x$ functionality (x = 2 and 3) in the case of $[(MDA)_2(MDA.2HCl)(H_2O)]$ (Figure 10(b)), and both are somewhat miscalculated. Table S5 lists the observed transition energies for MDA.HCl (6) and the calculated transition energies for $[(MDA)_2(MDA.2HCl)(H_2O)]$.

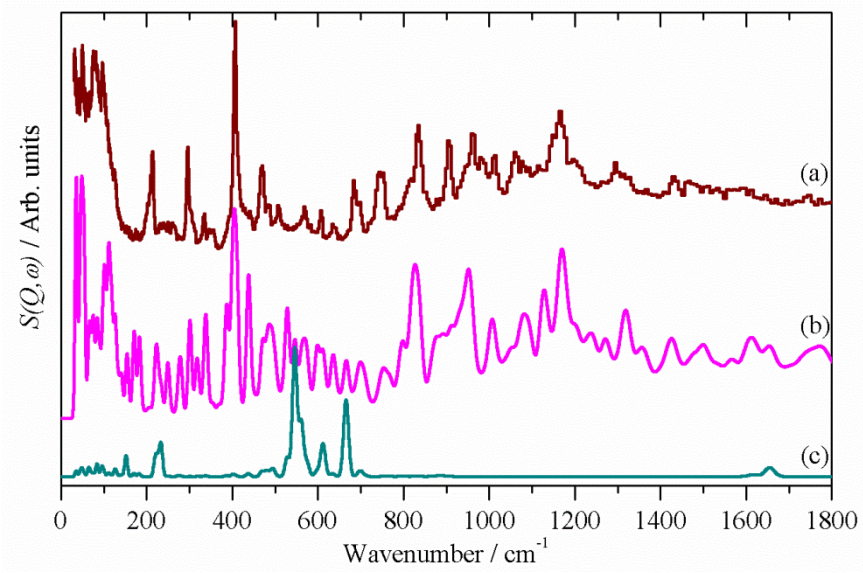

Figure 10. INS spectrum in the 0 – 1800 cm^{-1} range of (a) MDA.HCl (**6**), (b) the calculated spectrum for $[(MDA)_2(MDA.2HCl)(H_2O)]$ and (c) H_2O only.

4. Discussion

The vibrational spectra of amines has been extensively studied for many years and the characteristic group frequencies catalogued.[17-19] Most of these studies relate to the N–H stretching and bending modes; the other modes present have been much less studied. The reasons for this are as follows: (i) the low energy modes are often weak, (ii) they may be

obscured by other modes and (iii) some occur in the low energy region of the spectrum that is more difficult to access. INS spectroscopy in combination with *ab initio* calculations can alleviate some of these problems and the linear α,ω-alkanes $NH_2(CH_2)_nNH_2$ (*n* = 2–10,12), some alkyl polyamines and their hydrochloride salts have been studied by these methods.[7,8,20,21]

In the present work, we assign the vibrational spectra of the aromatic amines 4-BA (**1**) and MDA (**5**), their hydrochloride salts (4-BA.HCl (**2**), MDA.HCl (**6**), MDA.2HCl (**7**)) and the N-deuterated isotopomers (4-BA-D2 (**3**), 4-BA.DCl (**4**), MDA-D4 (**8**), MDA.2DCl (**9**)). The combination of INS and infrared spectroscopies allows the complete 0 – 4000 cm^{-1} spectroscopic range to be observed, and *ab initio* calculations of the periodic system allow the effects of the hydrogen bonding to be included. We note that the only previous computational study[22] of any of these molecules (MDA (**5**)) was for the isolated compound.

An isolated NH_2 group has nine degrees of freedom which manifest as three translations, three rotations and three internal vibrational modes. On attachment to a molecule (M), the three translations become an M–NH_2 stretch and two bending modes, if the molecule has a plane of symmetry *e.g.* an aromatic system, then these are in-plane and out-of-plane deformations. The three rotations become rock, wag and twist (torsion) modes, and the three internal vibrational modes remain as the scissors (H–N–H angle bend) and a symmetric (in-phase) and an asymmetric (out-of-phase) N–H stretch.

Similarly, for an NH_3 group, with 12 degrees of freedom, the three translations become an M–NH_3 stretch and in-plane and out-of-plane deformations (for an aromatic system). The three rotations become the torsion and a doubly degenerate rock and the six internal vibrational modes remain as a symmetric and a (doubly degenerate) asymmetric N–H bend and a

symmetric and an asymmetric (doubly degenerate) N–H stretch. (If the molecular symmetry is less than C_3 then the degeneracies will be lifted.)

Table 2 lists the modes that derive from the frustrated translations and rotations of the free NH_x group. It can be seen that the modes are reasonably well-reproduced by the calculations; the exception is the torsional mode which is over-estimated by 50 – 70 cm^{-1}. The reasons for this are not clear, but the origins presumably lie in the hydrogen bonding. Anharmonicity may also contribute to the discrepancy, but for this to be the sole cause would require an unusually large anharmonic component. We note that there are other examples where periodic-DFT over-estimates low energy modes involving hydrogen-bonding,[23-25]; these are particularly apparent in INS spectra as this is the region where the instruments perform best.

The intensity of a mode in the INS spectrum depends on the scattering cross section.[6] Modes involving particular atoms can be emphasised in the calculated spectra by giving them an arbitrarily large cross section and the remaining atoms zero cross section. Figure 11 shows the results for the all-hydrogen species where only the protons in the $–NH_x$ groups have non-zero cross section. As might be expected, the results for $[(MDA)_2(MDA.2HCl)(H_2O)]$ (Figure 11(e)) show features of both MDA (**5**) (Figure 11(c)) and MDA.2HCl (**7**) (Figure 11(d)).

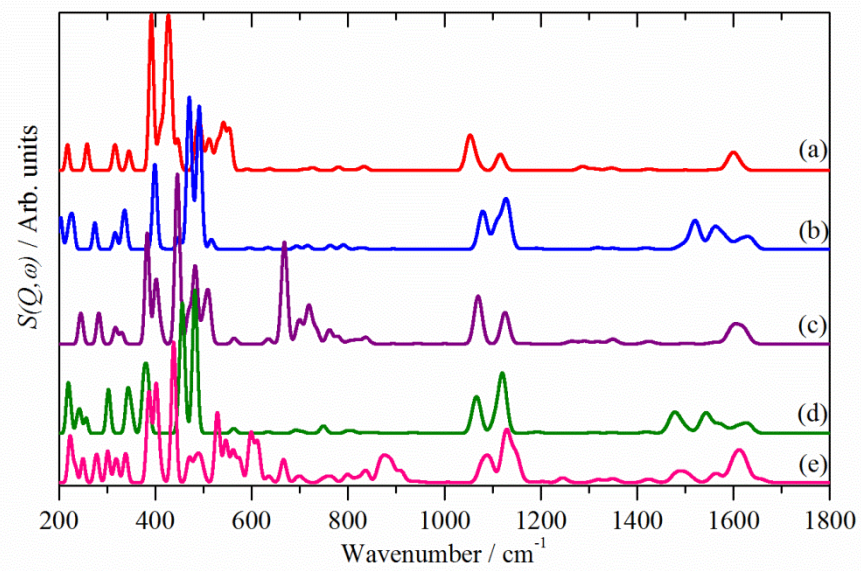

Figure 11. Calculated INS spectra of: (a) 4-BA (**1**), (b) 4-BA.HCl (**2**), (c) MDA (**5**), (d) MDA.2HCl (**7**) and (e) [$(MDA)_2(MDA.2HCl)(H_2O)$] in the 200 – 1800 cm^{-1} range.

Only the protons attached to nitrogen have non-zero cross section, thus the spectra emphasise modes of the $–NH_x$ groups. In this region, protonation of the amine functionality leads to only minor changes in the spectra. Thus the N–H bending modes at ~1600 cm^{-1} and the rocking modes at 1050 – 1150 cm^{-1} occur in similar ranges in all the compounds, only the torsion shows a clear shift to higher energy in the salts. This is in marked contrast to the N–H stretch region, where in the infrared spectra [3,4] (see Figure S1), the NH_2 modes are at 3400 – 3500 cm^{-1} and the NH_3 modes are at 2600 – 3000 cm^{-1} with much larger intensities. The CASTEP results can rationalise some of these observations. The N–H bond length is ~0.03 Å longer in the salts, which would reduce the transition energy. The static charges on the N-bonded hydrogens are the same in all the salts (Mulliken ~0.1 electron, Hirschfeld ~0.4 electron). However, components of the Born effective charges (which is a tensor and is defined as the electric polarization generated upon displacement of an atom, and thus are

dynamical charges) are three times larger in the salts, thus accounting for the greater infrared intensity.

The same procedure can be used to isolate the chloride modes (see Figure S5). In this case, there are no modes that are pure Cl^- translations; instead there are many modes where the chloride moves as the organic ions move.

In contrast, the water in the MDA.HCl complex, $[(MDA)_2(MDA.2HCl)(H_2O)]$, has distinct modes: translations at: 150, 220, 235 cm^{-1} and librations at: 546 (rock), 613 (twist) and 666 (wag) cm^{-1}. Assignment of the librational modes has long been recognised as problematic,[26,27] however, the combination of periodic-DFT and INS spectroscopy enables the modes to be observed and assigned. This approach has been previously used to assign the spectra of $LiOH.H_2O$,[28] in this case the order of the modes was wag ≈ twist > rock, similar to that found here, but in clear contradiction to the order predicted by the moments of inertia: rock > wag > twist.

5. Conclusions

The combination of periodic-DFT with infrared and INS spectroscopies has allowed the assignment of the spectra of a series of compounds[3, 4] that occur as unwanted by-products in the synthesis of the polyurethane precursor MDI or model compounds for these.

The model mono-amine derived aromatic compounds (**1-4**) enable useful comparisons between the free and protonated amine to be made, which define a comprehensive series of vibrational assignments and an assessment of relative band intensities. Developing these concepts further for the more technically relevant series of aromatic diamine compounds and their associated hydrochloride salts (**5-9**) then defines a more complete vibrational awareness for these molecules which are encountered in various commercial large-scale isocyanate

manufacturing process chains. For example, the infrared spectra allow a clear distinction in the N–H stretch region between the ionic salts and the parent amines. Moreover, in the fingerprint region, the calculations show that the transition energies of the $–NH_x$ deformation modes are surprisingly minimally changed by protonation of the amine group; the only exception is the torsion, which blue shifts by ~40 cm^{-1} in the salt, Table 2. This heightened understanding of the vibrational spectra, coupled with the feasibility of integrating infrared spectroscopy in to the process environment[5], provides new opportunities for in-line monitoring of the unit operation.

Supporting Information

Table S1: Mode descriptions, experimental and calculated vibrational transition energies of 4BA (**1**) and 4BA-D2 (**3**); Table S2: Mode descriptions, experimental and calculated vibrational transition energies of 4BA-HCl (**2**) and 4BA-DCl (**4**); Table S3: Mode descriptions, experimental and calculated vibrational transition energies of MDA (**5**) and MDA-D4 (**8**); Table S4: Mode descriptions, experimental and calculated vibrational transition energies of MDA-2HCl (**7**) and MDA-2DCl (**9**); Table S5: Mode descriptions: experimental (MDA-HCl (**6**)) and calculated $[(MDA)_2(MDA.2HCl)(H_2O)]$ vibrational transition energies; Figure S1. ^1H NMR spectra of 4-BA (**1**), 4-BA-D2 (**3**), 4-BA.HCl (**2**) and 4-BA.DCl (**4**); Figure S2. ^1H NMR spectra of MDA (**5**), MDA-D4 (**8**), MDA.2HCl (**7**) and MDA.2DCl (**9**); Figure S3. Infrared spectra of 4-BA (**1**), 4-BA.HCl (**2**); Figure S4. Infrared spectra of MDA (**5**), MDA.HCl (**6**) and MDA.2HCl (**7**); Figure S5. Calculated INS spectra of: (a) 4-BA.HCl (**2**), (b) MDA.2HCl (**7**) and (c) $[(MDA)_2(MDA.2HCl)(H_2O)]$ in the 0 – 300 cm^{-1} range.

Acknowledgements

The STFC Rutherford Appleton Laboratory is thanked for access to neutron beam facilities. Computing resources (time on the SCARF compute cluster for the CASTEP calculations) was provided by STFC's e-Science facility. Huntsman Polyurethanes are thanked for the provision of Ph.D. studentships (EKG, JC) and for project support.

References

1. Randall, D. Lee, S. *The Polyurethanes Book*, John Wiley, New York (**2002**).

2. Gibson, E. K; Winfield, J. M; Adam, D; Miller, A. A; Carr. R.H; Eaglesham. A; Lennon, D. The Solvation and Dissociation of 4-Benzylaniline Hydrochloride in Chlorobenzene. *Ind. Eng. Chem. Res.*, **2014**, *53*, 4156-4164.

3. Gibson, E.K; Winfield, J.M; Muir, K.W; Carr, R.H; Eaglesham, A; Gavezzotti, A; Lennon, D. A Structural and Spectroscopic Investigation of the Hydrochlorination of 4,4'-methylenedianiline, *Phys. Chem. Chem. Phys.*, **2010**, *12*, 3824-3833.

4. Gibson, E.K; Winfield, J.M; Muir, K.W; Carr, R.H; Eaglesham, A; Gavezzotti, A; Parker, S.F; D. Lennon, D. A Structural and Spectroscopic Investigation of the Hydrochlorination of 4-Benzylaniline: the Interaction of Anhydrous Hydrogen Chloride with Chlorobenzene, *Phys. Chem. Chem. Phys.*, **2009**, *11*, 288-297.

5. Chalmers, J.M; Dent, G. *Industrial Analysis with Vibrational Spectroscopy*, RSC Analytical Spectroscopy Monographs, Royal Society of Chemistry, Cambridge (**1997**).

6. Mitchell, P. C. H; Parker, S. F; Ramirez-Cuesta, A. J; Tomkinson, J; *Vibrational spectroscopy with neutrons, with applications in chemistry, biology, materials science and catalysis*, World Scientific, Singapore, **2005**

7. Marques, M. P. M; Batista de Carvalho, L. A. E; Tomkinson, J. Study of Biogenic and α,ω-Polyamines by Combined Inelastic Neutron Scattering and Raman Spectroscopies and by Ab Initio Molecular Orbital Calculations, *J. Phys. Chem. A*, **2002**, *106*, 2473-2482

8. Amado, A. M.; Otero, J. C.; Marques, M. P. M.; Batista de Carvalho, L. A. E. Spectroscopic and Theoretical Studies on Solid 1,2-Ethylenediamine Dihydrochloride Salt, *ChemPhysChem*, **2004**, *5*, 1837-1847

9. Parker, S. F.; Fernandez-Alonso, F.; Ramirez-Cuesta, A. J.; Tomkinson, J.; Rudic, S.; Pinna, R. S.; Gorini, G.; Fernández Castañon, J. Recent and Future Developments on TOSCA at ISIS, *J. Phys.: Conf. Ser.*, **2014**, *554*, 012003

10. http://www.isis.stfc.ac.uk/

11. Clark, S. J.; Segall, M. D.; Pickard, C. J.; Hasnip, P. J.; Probert, M. J.; Refson, K.; Payne, M.C. *Z.* First Principles Methods Using CASTEP, *Z. Kristallogr.* **2005**, *220,* 567-570

12. Refson, K.; Tulip, P. R.; Clark, S. J. Variational Density-Functional Perturbation Theory for Dielectrics and Lattice Dynamics, *Phys. Rev. B,* **2006**, *73*, 155114-155126

13. http://accelrys.com/products/materials-studio/

14. Jmol: an open-source Java viewer for chemical structures in 3D. http://www.jmol.org/

15. Ramirez-Cuesta, A. J. ACLIMAX 4.0.1, The New Version of the Software for Analyzing and Interpreting INS Spectra, *Comput. Phys. Commun.* **2004**, *157*, 226-238

16. Refson, K. *Phonons and Related Calculations in CASTEP*, http://www.castep.org/

17. Bellamy, L. J. *The Infrared Spectra of Complex Molecules*, 3rd Ed., Chapman and Hall, London, **1975**, ch. 14

18. Colthup, N. B; Daly, L. H; Wiberley, S. E. *Introduction to Infrared and Raman Spectroscopy*, 3rd Ed., Academic Press, San Diego, **1990**, ch. 11

19. Lin-Vien, D; Colthup, N. B; Fateley, W G; Grasselli, J. *The Handbook of Infrared and Raman Characteristic Frequencies of Organic Molecules*, Academic Press, Boston, **1991**, ch. 10.

20. Batista de Carvalho, L. A. E; Marques, M. P. M; Tomkinson, J. Transverse Acoustic Modes of Biogenic and α,ω-Polyamines: A Study by Inelastic Neutron Scattering and Raman Spectroscopies Coupled to DFT Calculations, *J. Phys. Chem. A*. **2006**, *110*, 12947-12954

21. Batista de Carvalho, L. A. E; Marques, M. P. M. Vibrational Spectroscopy Studies on Linear Polyamines, *Biochem. Soc. Trans.* **2007**, *35*, 374-380

22. Badawi, H. M. A Comparative Study of the Structure and Vibrational Spectra of Diphenylmethane, the Carcinogen 4,4'-Methylenedianiline and 4,4'-Methylenebis(N,N-Dimethylaniline), *Spectrochim. Acta, Part A*, **2013**, *109*, 213-220

23. Tian, L; Kolesnikov, A. I; Li, J; Ab Initio Simulation of Hydrogen Bonding in Ices Under Ultra-High Pressure, *J. Chem. Phys.* **2012**, *137*, 204507-204511

24. Zhang, P; Tian, L; Zhang, Z. P; Shao, G; Li, J. Investigation of the Hydrogen Bonding in Ice Ih by First-Principles Density Function Methods, *J. Chem. Phys.* **2012**, *137*, 044504-044509

25. Albers, P. W; Glenneberg, J; Refson K; Parker, S. F. Inelastic Incoherent Neutron Scattering Study of the Molecular Properties of Pure Hydrogen Peroxide and its Water Mixtures of Different Concentration, *J. Chem. Phys.* **2014**, *140*, 164504-164514

26. Tayal, V. P.; Srivastava, B. K.; Khandelwal, D. P. Librational Modes of Crystal Water in Hydrated Solids, *Appl. Spectrosc. Rev.* **1980**, *16*, 43-134

27. Lutz, H. D. Bonding and Structure of Water Molecules in Solid Hydrates – Correlation of Spectroscopic and Structural Data, *Struct. Bonding (Berlin, Ger.)*, **1988**, *69*, 97-125

28. Parker, S. F.; Refson, K.; Bewley R. I.; Dent, G. Assignment of the Vibrational Spectra of Lithium Hydroxide Monohydrate, $LiOH \cdot H_2O$, *J. Chem. Phys.* **2011**, *134*, 084503-084510

Table 1: Comparison of experimental and calculated geometries of 4-BA (**1**), 4-BA.HCl (**2**), MDA (**5**), MDA.2HCl (**7**) and [$(MDA)_2(MDA.2HCl)(H_2O)$] (Distances in Å and angles (∠) in degrees).

	4-BA		4-BA.HCl		MDA		MDA.2HCl		$[(MDA)_2(MDA.2HCl)(H_2O)]$		
	Expt	Calc	Expt	Calc	Expt	Calc	Expt	Calc	Expt	Calc	
N–H (ave)	0.926	1.019			0.921	1.023			0.879	1.028	(NH_2)
			0.926	1.058			0.872	1.056	0.915	1.057	(NH_3)
sp^2C–H	0.950	1.092			0.950	1.091			0.950	1.091	(NH_2)
(ave)			0.950	1.090			0.950	1.090	0.950	1.090	(NH_3)
sp^3C–H	0.990	1.101			0.990	1.103			0.990	1.102	(NH_2)
(ave)			0.990	1.101			0.990	1.099	0.991	1.102	(NH_3)
Ring–CH_2	1.512,	1.513,	1.510,	1.509,	1.513,	1.509,	1.511	1.513	1.513,1.521	1.512,1.520	(NH_2)
	1.521	1.518	1.521	1.517	1.523	1.520			1.516	1.511	(NH_3)
Ring–N	1.388	1.393			1.397, 1.409	1.389, 1.409			1.420,1.423	1.422,1.424	(NH_2)
			1.470	1.472			1.472	1.469	1.463	1.465	(NH_3)

$sp^2C–sp^2C$	1.391	1.401			1.386	1.402			1.393	1.399	(NH_2)
(ave)			1.385	1.397			1.382	1.396	1.390	1.396	(NH_3)
∠ Ring–	112.4	112.8	114.7	114.9	115.6	115.1	112.9	112.6	115.7	115.2	(NH_2)
CH_2–Ring									114.3	114.4	(NH_3)
∠ Ring	126.2	125.6	150.9	151.1	162.7	159.3	109.2	108.1	136.5	136.1	(NH_2)
dihedral									142.3	142.3	(NH_3)
N•••N	3.875	3.958			3.172	3.096			2.869	2.841	
N•••Cl			3.157	3.157			3.233	3.193	3.196	3.216	
O–H									0.909	0.985	
O•••Cl									3.118	3.086	
∠ H–O–H									96.3	102.0	

Table 2: Compilation of the observed and calculated transition energies (cm^{-1}) of the frustrated translations and rotations of the $–NH_x$ moieties.

	Translations						Rotations					
	NH_x out-of-plane bend		NH_x in-plane bend		M–NH_x stretch		NH_x torsion		NH_2 wag		NH_x rock	
	Obs	Calc[a]	Obs	Calc	Obs	Calc	Obs	Calc	Obs	Calc	Obs	Calc
4-BA	314	316	403	392	1283	1287	354	428	521	536		1053
4-BA.HCl	338	336		399	1202	1191/1202	401	474	–	–	1077	1081
MDA	321/334	318/331		384/402	1269/1287	1265/1290	380/397	446/478	612/760	699/724	1070/1080	1068/1073
MDA.2HCl	341	345	375	381	1206	1196	419	470	–	–	1069	1065

[a]Average of factor group components

Table of Contents entry